



The skin is a significant but overlooked anatomical reservoir for vector-borne African trypanosomes

Paul Capewell, Christelle Cren-Travaillé, Francesco Marchesi, Pamela Johnston, Taylor-Anne Gorman, Estefania Calvo-Alvarez, Aline Crouzols, Grégory Jouvion, Vincent Jammoneau, William Weir, et al.

► **To cite this version:**

Paul Capewell, Christelle Cren-Travaillé, Francesco Marchesi, Pamela Johnston, Taylor-Anne Gorman, et al.. The skin is a significant but overlooked anatomical reservoir for vector-borne African trypanosomes. eLife, eLife Sciences Publication, 2016, <10.7554/eLife.17716>. <pasteur-01371190>

HAL Id: pasteur-01371190

<https://hal-pasteur.archives-ouvertes.fr/pasteur-01371190>

Submitted on 24 Sep 2016

HAL is a multi-disciplinary open access archive for the deposit and dissemination of scientific research documents, whether they are published or not. The documents may come from teaching and research institutions in France or abroad, or from public or private research centers.

L'archive ouverte pluridisciplinaire **HAL**, est destinée au dépôt et à la diffusion de documents scientifiques de niveau recherche, publiés ou non, émanant des établissements d'enseignement et de recherche français ou étrangers, des laboratoires publics ou privés.



Distributed under a Creative Commons Attribution 4.0 International License

1 **The skin is a significant but overlooked anatomical reservoir for vector-borne African**
2 **trypanosomes**

3

4 Paul Capewell^{1*}, Christelle Cren-Travaillé^{2*}, Francesco Marchesi³, Pamela Johnston³, Caroline
5 Clucas¹, Robert A Benson⁴, Taylor-Anne Gorman^{1,4}, Estefania Calvo-Alvarez², Aline Crouzols²,
6 Grégory Jouvion⁵, Vincent Jammoneau⁶, William Weir¹, M Lynn Stevenson³, Kerry O'Neill¹, Anneli
7 Cooper¹, Nono-raymond Kuispond Swar⁷, Bruno Bucheton⁶, Dieudonné Mumba Ngoyi⁸, Paul
8 Garside⁴, Brice Rotureau^{2**} and Annette MacLeod^{1**}

9

10 ¹Wellcome Trust Centre for Molecular Parasitology, College of Medical, Veterinary and Life
11 Sciences, Henry Wellcome Building for Comparative Medical Sciences, Garscube Estate, Glasgow,
12 United Kingdom, G61 1QH

13 ²Trypanosome Transmission Group. Trypanosome Cell Biology Unit, INSERM U1201 & Department
14 of Parasites and Insect Vectors, Institut Pasteur, Paris, France

15 ³Veterinary Diagnostic Services, Veterinary School, University of Glasgow, Garscube Estate,
16 Glasgow, United Kingdom, G61 1QH

17 ⁴Institute of Infection, Immunology and Inflammation, College of Medical, Veterinary and Life
18 Sciences, Glasgow Biomedical Research Centre, University of Glasgow, Glasgow, United Kingdom,
19 G12 8TA

20 ⁵Human Histopathology and Animal Models Unit, Institut Pasteur, Paris, France

21 ⁶Institut de Recherche pour le Développement, Unité Mixte de Recherche IRD-CIRAD 177, Campus
22 International de Baillarguet, Montpellier, France

23 ⁷University of Kinshasa, Kinshasa, Democratic Republic of the Congo

24 ⁸Department of Parasitology, National Institute of Biomedical Research (INRB), Kinshasa,
25 Democratic Republic of the Congo

26

27 * Joint first authors

28 ** Joint last authors

29 **The authors have no competing financial interests.**

30 **Keywords**

31 Skin, blood, reservoir, transmission, infection, Human African Trypanosomiasis, trypanosomes,
32 *Trypanosoma brucei*, tsetse fly, vector-borne, evolution

33

34 **Abstract**

35 The role of mammalian skin in harbouring and transmitting arthropod-borne protozoan parasites has
36 been overlooked for decades as these pathogens have been regarded primarily as blood-dwelling
37 organisms. Intriguingly, infections with low or undetected blood parasites are common, particularly
38 in the case of Human African Trypanosomiasis caused by *Trypanosoma brucei gambiense*. We
39 hypothesise, therefore, the skin represents an anatomic reservoir of infection. Here we definitively
40 show that substantial quantities of trypanosomes exist within the skin following experimental
41 infection, which can be transmitted to the tsetse vector, even in the absence of detectable
42 parasitaemia. Importantly, we demonstrate the presence of extravascular parasites in human skin
43 biopsies from undiagnosed individuals. The identification of this novel reservoir requires a re-
44 evaluation of current diagnostic methods and control policies. More broadly, our results indicate that
45 transmission is a key evolutionary force driving parasite extravasation that could further result in
46 tissue invasion-dependent pathology.

47

48 **Introduction**

49 Understanding the process of parasite transmission is essential for the design of rational control
50 measures to break the disease cycle and requires the identification of all reservoirs of infection. In a
51 number of vector-borne diseases, it is becoming evident that asymptomatic individuals, be they
52 humans or animals, can represent a significant proportion of the infected population and therefore
53 an important reservoir of disease that requires targeting by control measures¹⁻⁴. The recent
54 identification in West Africa of asymptomatic individuals with human trypanosomiasis (long-term
55 seropositives) but undetected parasitaemia, raises the question of what role these individuals play
56 in disease transmission^{3,5-7}. Therapy is currently only directed towards microscopy-positive
57 individuals and thus a proportion of the infected population remain untreated.

58 There is convincing evidence that seropositive individuals with low or undetected parasitaemia
59 contain transmissible trypanosomes. Xenodiagnosis experiments, in which tsetse flies are fed on
60 microscopy-negative infected humans⁸ or, more recently, experimentally-infected pigs⁹, have shown
61 that these apparently aparasitaemic hosts contain the parasite since the tsetse flies became
62 infected. It is uncertain where the trypanosomes reside in the host but, given the telmophagus
63 (slash and suck) feeding habit of the tsetse fly, they could be skin-dwelling parasites ingested with
64 the blood meal. Our findings suggest that parasites may be sufficiently abundant in the skin to allow
65 transmission and therefore the skin may represent an anatomical reservoir of infection.

66 Detection of trypanosomes in the skin is not well documented, although there are descriptions of
67 cutaneous symptoms associated with African trypanosomiasis and distinct 'trypanid' skin lesions¹⁰.
68 Imaging data from mouse models of infection suggest that trypanosomes sequester to major organs
69 such as the spleen, liver and brain^{11,12} and recent evidence has demonstrated trypanosomes in
70 extravascular adipose tissue¹³. These adipose-associated trypanosomes appear to be a new life-
71 cycle stage with a distinct transcriptional profile and, while tsetse bite-site associated transmission
72 has been suggested¹⁴, and a historical study made a passing observation of localised deposition of
73 trypanosomes in the skin matrix¹⁵, the broader role of skin-dwelling trypanosomes in transmission
74 remains unclear. In this paper we report the investigation of a possible anatomical reservoir in the
75 skin of the mammalian host. We provide conclusive evidence of *T.b. brucei*, (a causative agent of
76 animal trypanosomiasis) and the human-infective trypanosome, *T.b. gambiense*, invading the
77 extravascular tissue of the skin (including but not restricted to the adipose tissue) and undergoing
78 onward transmission despite undetected vascular parasitaemia. We also provide evidence of
79 localisation of trypanosomes within the skin of undiagnosed humans. The presence of a significant
80 transmissible population of *T. brucei* in this anatomical compartment is likely to impact future control
81 and elimination strategies for both animal and human trypanosomiases.

82

83 Results

84 In order to investigate the potential for extravascular skin invasion by *T. brucei*, BALB/c mice were
85 inoculated via IP injection with the low virulence STIB247 strain of *T. brucei* and skin sections were
86 assessed over a 36-day time-course. The presence and relative quantities of extravascular
87 parasites were evaluated by semi-quantitative scoring of the histological samples (Figure 1-source
88 data 1) and compared to blood parasitaemia (Figure 1-source data 2). Extravascular parasites were
89 first observed in the skin 12 days post-infection and remained throughout the experiment. Skin
90 parasite numbers fluctuated to a lesser extent than blood parasitaemia and the apparent periodicity
91 in the skin may be due to one particularly high data point on day 24 (Figure 1). Parasites were found
92 in the dermis, subcutaneous adipose tissue (Figure 2) and in fascia beneath the panniculus
93 carnosus muscle. We did not detect any particular clustering around dermal adipocytes. The
94 presence of parasites in the skin was not associated with major inflammation (Supplementary File
95 1). To confirm that skin invasion by this parasite was not strain or sub-species specific, the more
96 virulent TREU927 strain of *T. brucei* and the human-infective *T.b. gambiense* strain, PA, were used
97 to infect mice. Extravascular skin invasion of the dermis, subcutaneous adipose tissue and fascial
98 planes (Figure 2-figure supplement 1) was evident with associated mild to moderate inflammation
99 (Supplementary File 2), in some instances the degree of skin invasion in the *T.b. gambiense*
100 infected mice was far greater than *T.b. brucei*, perhaps suggesting a greater propensity for
101 sequestration in this sub-species.

102 To confirm that the extravascular distribution of parasites was not an artefact of the route of
103 inoculation, infections by natural vector transmission were carried out using a bioluminescent *T.b.*
104 *brucei* strain, AnTat1.1E AMLuc/tdTomato. Mice were infected by a single infective bite of an
105 individual *G.m. morsitans*. After 4 to 11 days and up to the end of the experiment, parasites were
106 observed in the skin with a dynamic distribution (Figure 3A) and a variable density (Figure 3B).
107 Parasites were first detected in the blood between 5 and 19 days after natural transmission and
108 parasitaemia remained lower than 10^7 parasites/ml. Observed bioluminescence directly reflects the
109 total number of living parasites in the entire organism, including blood and viscera, but the intensity
110 of the signal decreases with tissue depth. Therefore, at the end of each experiment, mice were
111 sacrificed and their organs were checked for bioluminescence. The presence of extravascular
112 parasites in cutaneous and subcutaneous tissues was first demonstrated by bioluminescence
113 imaging in entire dissected skins (Figure 3C) and was not necessarily localised to the bite site. In
114 addition to the skin, only the spleen, some lymph nodes and adipose tissue were observed to be
115 positive for bioluminescence in several individuals (Figure 3-figure supplement 1). This suggests
116 that the observed bioluminescence is likely to originate predominantly, but not solely, from parasites
117 in the skin. In addition, only mild inflammation was observed after 29 days (Figure 3-figure
118 supplement 2).

119 To confirm that trypanosomes in the skin are a viable population, fluorescent parasites were
120 monitored by two intravital imaging methods following IP injection and natural transmission (Figure
121 4). First, IP-injected fluorescent *T. brucei* STIB247 were imaged *in vivo* using 2-photon microscopy
122 (Figure 4A). Extravascular trypanosomes observed in the dermal layer of dorsal skin were highly
123 motile, consistent with viability (Video 1). Second, naturally-transmitted fluorescent *T. brucei*
124 AnTat1.1E AMLuc/tdTomato were imaged *in vivo* using spinning-disk confocal microscopy in the
125 C57BL/6J-Flk1-EGFP mouse line that has green fluorescent endothelial cells in the lymphatic and
126 blood vessels¹⁶ (Figure 4B). Extravascular trypanosomes were observed in the dermal layer of the
127 ear and were highly motile (Videos 2, 3 and 4).

128 Differentiation of dividing trypanosomes to non-dividing stumpy forms is essential for transmission to
129 the tsetse. Using the relative transcript abundance of the stumpy marker Protein Associated with
130 Differentiation 1 (PAD1)¹⁷ to an endogenous control, Zinc Finger Protein 3 (ZFP3)¹⁸, we estimated
131 that approximately 20% of skin-dwelling parasites were stumpy (Supplementary File 3). To directly
132 determine the proportion of stumpy forms in skin sections, histological staining for PAD1 was also
133 performed (Table 1-source data 4). PAD1-positive cells were observed in variable proportions (from
134 8 to 80%) in all bioluminescent skin samples examined after IP injection (Supplementary File 4).
135 Following natural transmission, up to 38% of parasites detected using VSG surface markers (Figure
136 3-figure supplement 3A-B) also expressed PAD1 (Figure 3-figure supplement 3C-D) (n=441 cells
137 from 8 skin sections). In all skin sections, stumpy parasites were homogeneously distributed in the
138 dermis and subcutaneous adipose tissues.

139 We next assessed the ability of skin-dwelling parasites to infect tsetse flies. Teneral flies (immature
140 flies that have not yet taken a blood meal) were fed on different regions of skin from mice infected
141 with AnTat1.1E AMLuc/TY1/tdTomato with differing levels of bioluminescence across the skin
142 (Table 1-source data 1 and Table 1-source data 2). This was repeated in 20 mice with differing
143 levels of parasitaemia. Flies were dissected and checked for the presence of fluorescent
144 trypanosomes after two days (Table 1). In mice with undetectable or low parasitaemia ($<5 \times 10^4$
145 parasites/ml), no parasites were found in flies fed on non-bioluminescent regions. Conversely, a
146 median of 36% ($\pm 23\%$, n=70) of flies that fed on bioluminescent regions of low parasitaemic mice
147 became infected (Table 1 and Table 1-source data 3). This demonstrates that skin parasites, from
148 mice without visible parasitaemia, can contribute to tsetse infection, possibly reflecting human
149 asymptomatic infections. When parasites were detected in the blood and skin, tsetse infection rates
150 increased up to 100% (median of 61% $\pm 22\%$, n=120) (Table 1 and Table 1-source data 3).
151 Parasites taken-up from the skin were able to further develop through the life-cycle to early procyclic
152 forms in the fly as evidenced by GPEET-procyclicin marker on the parasites surface (n=721 cells from
153 16 flies) (Table 1-source data 4 and Supplementary File 4).

154 To demonstrate that skin invasion by trypanosomes can occur in humans as well as the murine
155 model, slides of historical skin biopsies, taken as part of a diagnostic screening programme for

156 *Onchocerca* microfilaria in the trypanosomiasis-endemic Democratic Republic of the Congo, were
157 examined for trypanosomes. At the time of sampling, the incidence of trypanosomiasis was 1.5-2%
158 and we hypothesised that some individuals may have harboured undiagnosed infections. Re-
159 examination of 1,121 skin biopsies by microscopy revealed six individuals with trypanosomes in
160 their skin (Figure 5). These individuals had not previously been diagnosed with human
161 trypanosomiasis by clinical signs or the presence of blood parasites.

162

163 **Discussion**

164 We have shown that there exists a significant yet overlooked population of live, motile,
165 extravascular *T. brucei* in the dermis and subcutis of animal models infected by artificial routes or by
166 vector transmission. It is likely that once injected the parasites disseminate via the lymph and blood
167 to the skin where they are ingested during tsetse fly pool-feeding and readily initiate cyclical
168 development in the vector. Given the relative volume of the skin organ compared to the vasculature,
169 it is possible, depending on the density of skin invasion, that more parasites exist in the skin than in
170 the blood. The skin, therefore, represents an unappreciated reservoir of infection. The extravasation
171 of trypanosomes was described previously in major organs such as liver, spleen^{11,12} and visceral
172 adipose tissue¹³, but the importance of these parasites in transmission was not investigated. Here
173 we show that these skin-dwelling trypanosomes contribute to transmission and could explain the
174 maintenance of disease foci, despite active screening and treatment. Skin invasion for enhanced
175 transmission is likely a powerful evolutionary force driving extravasation, suggesting that the
176 generalised tissue penetration underlying pathogenesis (i.e. splenomegaly, hepatomegaly, CNS
177 invasion) is a secondary epiphenomenon. A skin reservoir also presents a novel target for
178 diagnostics (e.g. skin biopsies), allowing the prevalence of infection to be accurately determined
179 and the identification of any previously undetected animal reservoirs of human disease.

180 The skin as an anatomical reservoir of parasites is a recurring theme in arthropod-borne human
181 diseases such as *Leishmania*^{19,20} and *Onchocerca*^{21,22}. Here we present evidence of trypanosomes
182 in the skin of hitherto undiagnosed individuals. This anatomical reservoir may serve to explain how
183 HAT foci re-emerge and persist despite low numbers of reported cases even in the absence of an
184 animal reservoir²³⁻²⁵.

185 HAT was once widespread across much of sub-Saharan Africa but concerted control efforts brought
186 it close to elimination during the 1960s^{26,27}. However, disease foci persisted, with a resurgence in
187 the number of reported cases to over 300,000 in the 1990s²⁶⁻²⁸. Currently, HAT is approaching
188 elimination in many areas^{27,29}. Understanding how HAT evaded elimination in the latter half of the
189 20th century and how it continues to persist is vital to efforts to eliminate the disease. For example,
190 our results indicate that it may be necessary to develop novel therapeutics capable of accessing
191 extravascular compartments. The current policy in most endemic countries is not to treat
192 serologically positive individuals unless they demonstrate active infection, due to the long duration

193 and high toxicity of treatment and the low predictive value of the serological tests. We suggest that
194 this policy should be reconsidered in light of our compelling evidence that they represent a carrier
195 population which may maintain HAT foci and explain previously thwarted efforts to eliminate this
196 major pathogen.

197 **Acknowledgments**

198 We acknowledge P. Solano, D. Engman, K. Matthews, M. Taylor, M. Carrington, R. Amino, E.
199 Myburgh and K. Gull for providing various material, cell lines, antibodies and plasmids and to A. Tait
200 for critically reviewing this manuscript.

201 **References**

- 202 1. Lindblade, K. A., Steinhardt, L., Samuels, A., Kachur, S. P. & Slutsker, L. The silent threat:
203 asymptomatic parasitemia and malaria transmission. *Expert Review of Anti-infective Therapy*
204 **11**, 623–639 (2014).
- 205 2. Fakhar, M. *et al.* Asymptomatic human carriers of *Leishmania infantum*: possible reservoirs
206 for Mediterranean visceral leishmaniasis in southern Iran. *Annals of Tropical Medicine &*
207 *Parasitology* **102**, 577–583 (2013).
- 208 3. Koffi, M. *et al.* Aparasitemic serological suspects in *T. b. gambiense* human African
209 trypanosomiasis: A potential human reservoir of parasites? *Acta Tropica* **98**, 183–188 (2006).
- 210 4. Berthier, D. *et al.* Tolerance to Trypanosomatids: A Threat, or a Key for Disease Elimination?
211 *Trends in Parasitology* **32**, 157–168 (2016).
- 212 5. Jamonneau, V. *et al.* Untreated human infections by *Trypanosoma brucei gambiense* are not
213 100% fatal. *PLoS Neglected Tropical Diseases* **6**, e1691 (2012).
- 214 6. Bucheton, B., MacLeod, A. & Jamonneau, V. Human host determinants influencing the
215 outcome of *Trypanosoma brucei gambiense* infections. *Parasite Immunol.* **33**, 438–447
216 (2011).
- 217 7. Kanmogne, G. D., Asonganyi, T. & Gibson, W. C. Detection of *T. brucei gambiense*, in
218 serologically positive but aparasitaemic sleeping-sickness suspects in Cameroon, by PCR.
219 *Ann Trop Med Parasitol* **90**, 475–483 (1996).
- 220 8. Frezil, J. L. [Application of xenodiagnosis in the detection of *T. gambiense* trypanosomiasis in
221 immunologically suspect patients]. *Bull Soc Pathol Exot Filiales* **64**, 871–878 (1971).
- 222 9. Wombou Toukam, C. M., Solano, P., Bengaly, Z., Jamonneau, V. & Bucheton, B.
223 Experimental evaluation of xenodiagnosis to detect trypanosomes at low parasitaemia levels
224 in infected hosts. *Parasite* **18**, 295–302 (2011).
- 225 10. McGovern, T. W. *et al.* Cutaneous manifestations of African trypanosomiasis. *Arch Dermatol*
226 **131**, 1178–1182 (1995).
- 227 11. Blum, J. A., Zellweger, M. J., Burri, C. & Hatz, C. Cardiac involvement in African and
228 American trypanosomiasis. *Lancet Infect Dis* **8**, 631–641 (2008).
- 229 12. Kennedy, P. G. E. Human African trypanosomiasis of the CNS: current issues and
230 challenges. *Journal of Clinical Investigation* **113**, 496–504 (2004).
- 231 13. Trindade, S. *et al.* *Trypanosoma brucei* parasites occupy and functionally adapt to the
232 adipose tissue in mice. *Cell Host & Microbe* (2016).
- 233 14. Caljon, G. *et al.* The Dermis as a Delivery Site of *Trypanosoma brucei* for Tsetse Flies. *PLoS*
234 *Pathogens* **12**, e1005744 (2016).
- 235 15. Goodwin, L. G. Pathological effects of *Trypanosoma brucei* on small blood vessels in rabbit
236 ear-chambers. *Trans. R. Soc. Trop. Med. Hyg.* **65**, 82–88 (1971).
- 237 16. Ema, M., Takahashi, S. & Rossant, J. Deletion of the selection cassette, but not cis-acting
238 elements, in targeted Flk1-lacZ allele reveals *Flk1* expression in multipotent mesodermal

- 239 progenitors. *Blood* **107**, 111–117 (2006).
- 240 17. Dean, S., Marchetti, R., Kirk, K. & Matthews, K. R. A surface transporter family conveys the
241 trypanosome differentiation signal. *Nature* **459**, 213–217 (2009).
- 242 18. Walrad, P., Paterou, A., Acosta-Serrano, A. & Matthews, K. R. Differential Trypanosome
243 Surface Coat Regulation by a CCCH Protein That Co-Associates with procyclin mRNA cis -
244 Elements. *PLoS Pathogens* **5**, e1000317 (2009).
- 245 19. Sacks, D. in *Leishmania After the Genome* (2008).
- 246 20. Schlein, Y. *Leishmania* and sandflies: interactions in the life cycle and transmission.
247 *Parasitol. Today (Regul. Ed.)* (1993). doi:10.1016/0169-4758(93)90070-V
- 248 21. Onchocerciasis. Symptomatology, pathology, diagnosis. (1974).
- 249 22. Dalmat, H. T. in *Onchocerciasis* 425 (1955).
- 250 23. Kagbadouno, M. S. *et al.* Epidemiology of sleeping sickness in Boffa (Guinea): where are the
251 trypanosomes? *PLoS Neglected Tropical Diseases* **6**, e1949 (2012).
- 252 24. Cordon-Obras, C. *et al.* *Trypanosoma brucei gambiense* in domestic livestock of Kogo and
253 Mbini foci (Equatorial Guinea). *Tropical Medicine and International Health* **14**, 535–541
254 (2009).
- 255 25. Balyeidhusa, A. S. P., Kironde, F. A. S. & Enyaru, J. C. K. Apparent lack of a domestic animal
256 reservoir in *Gambiense* sleeping sickness in northwest Uganda. *Veterinary Parasitology* **187**,
257 157–167 (2012).
- 258 26. World Health Organization. Dept. of Epidemic, Alert, P.Response. WHO report on global
259 surveillance of epidemic-prone infectious diseases. (2000).
- 260 27. World Health Organization. Control and surveillance of human African trypanosomiasis.
261 *World Health Organ Tech Rep Ser* 1–237 (2013).
- 262 28. Steverding, D. The history of African trypanosomiasis. *Parasites Vectors* **1**, 3 (2008).
- 263 29. Simarro, P. P. *et al.* Estimating and Mapping the Population at Risk of Sleeping Sickness.
264 *PLoS Neglected Tropical Diseases* **6**, e1859 (2012).
- 265 30. Geigy, R., Kauffmann, M. & Jenni, L. Wild mammals as reservoirs for Rhodesian sleeping
266 sickness in the Serengeti, 1970-71. *Trans. R. Soc. Trop. Med. Hyg.* **67**, 284–286 (1973).
- 267 31. Goedbloed, E. *et al.* Serological studies of trypanosomiasis in East Africa. II. Comparisons of
268 antigenic types of *Trypanosoma brucei* subgroup organisms isolated from wild tsetse flies.
269 *Ann Trop Med Parasitol* **67**, 31–43 (1973).
- 270 32. Tait, A., Babiker, E. A. & Le Ray, D. Enzyme variation in *Trypanosoma brucei* ssp. I Evidence
271 for the sub-speciation of *Trypanosoma brucei gambiense*. *Parasitology* **89**, 311–326 (1984).
- 272 33. Myburgh, E. *et al.* In vivo imaging of trypanosome-brain interactions and development of a
273 rapid screening test for drugs against CNS stage trypanosomiasis. *PLoS Neglected Tropical*
274 *Diseases* **7**, e2384 (2013).
- 275 34. Le Ray, D., Barry, J. D., Easton, C. & Vickerman, K. First tsetse fly transmission of the
276 'AnTat' serodeme of *Trypanosoma brucei*. *Ann Soc Belg Med Trop* (1977).
- 277 35. Xong, H. V. *et al.* A VSG expression site-associated gene confers resistance to human serum
278 in *Trypanosoma rhodesiense*. *Cell* **95**, 839–846 (1998).
- 279 36. Fragoso, C. M. & Roditi, I. Highly efficient stable transformation of bloodstream forms of
280 *Trypanosoma brucei*. *Mol Biochem Parasitol* **153**, 220–223 (2007).
- 281 37. Branchini, B. R., Southworth, T. L., Khattak, N. F., Michelini, E. & Roda, A. Red- and green-
282 emitting firefly luciferase mutants for bioluminescent reporter applications. *Anal. Biochem.*
283 **345**, 140–148 (2005).
- 284 38. Bastin, P., Bagherzadeh, Z., Matthews, K. R. & Gull, K. A novel epitope tag system to study
285 protein targeting and organelle biogenesis in *Trypanosoma brucei*. *Mol Biochem Parasitol* **77**,
286 235–239 (1996).
- 287 39. Magez, S. & Caljon, G. Mouse models for pathogenic African trypanosomes: unravelling the
288 immunology of host-parasite-vector interactions. *Parasite Immunol.* **33**, 423–429 (2011).
- 289 40. Lumsden, W. H. Quantitative methods in the study of trypanosomes and their applications:
290 With special reference to diagnosis. *Bull. World Health Organ.* **28**, 745–752 (1963).
- 291 41. Rotureau, B., Subota, I., Buisson, J. & Bastin, P. A new asymmetric division contributes to
292 the continuous production of infective trypanosomes in the tsetse fly. *Development* **139**,
293 1842–1850 (2012).

- 294 42. MacGregor, P., Savill, N. J., Hall, D. & Matthews, K. R. Transmission Stages Dominate
295 Trypanosome Within-Host Dynamics during Chronic Infections. *Cell Host & Microbe* **9**, 310–
296 318 (2011).
- 297 43. Zamze, S. E., Ferguson, M. A., Collins, R., Dwek, R. A. & Rademacher, T. W.
298 Characterization of the cross-reacting determinant (CRD) of the glycosyl-phosphatidylinositol
299 membrane anchor of *Trypanosoma brucei* variant surface glycoprotein. *Eur. J. Biochem.* **176**,
300 527–534 (1988).
- 301 44. Kohl, L., Sherwin, T. & Gull, K. Assembly of the paraflagellar rod and the flagellum
302 attachment zone complex during the *Trypanosoma brucei* cell cycle. *J. Eukaryot. Microbiol.*
303 **46**, 105–109 (1999).
- 304 45. Makenga Bof, J. C. *et al.* Onchocerciasis control in the Democratic Republic of Congo (DRC):
305 challenges in a post-war environment. *Tropical Medicine and International Health* **20**, 48–62
306 (2015).
- 307
308

309 **Methods**

310 **Trypanosome strains and cultures**

311 All strains used in this study are pleomorphic. STIB247 is a low virulence *T.b. brucei* strain that
312 induces a chronic infection and was isolated from a hartebeest in the Serengeti in 1971³⁰. TREU927
313 is the genome reference strain for *T. brucei* and is more virulent than STIB247. This strain was
314 isolated from a tsetse fly in Kenya in 1969/1970³¹. PA is a human-infective group 1 *T.b. gambiense*
315 strain isolated from a patient in the Democratic Republic of the Congo in 1975³². mCherry STIB247
316 was created by transfection of STIB247 with pHD1034-mCherry³³. This strain constitutively
317 expresses fluorescent mCherry from the ribosomal RNA promoter and its expression is stable over
318 repeated passage.

319 The AnTat 1.1E clone of *T.b. brucei* was derived from a strain originally isolated from a bushbuck in
320 Uganda in 1966³⁴. Bloodstream forms were cultivated in HMI11 medium supplemented with 10%
321 foetal calf serum at 37°C in 5% CO₂. This strain was genetically engineered to produce two strains
322 continuously expressing the red-shifted luciferase (PpyRE9H) and the tdTomato red fluorescent
323 protein either individually or in combination.

324 For the first AnTat 1.1E strain, the pTbAMLuc plasmid (M. Taylor, London School of Hygiene and
325 Tropical Medicine, UK) was used for continuous cytosolic expression of the red-shifted luciferase
326 PpyRE9H. The tdTomato coding sequence was cloned with *HindIII* and *BamHI* into the pTSARib
327 vector³⁵, generating the final pTSARib-tdTomato construct. The two plasmids were linearised with
328 *KpnI* and *SphI* restriction enzymes, respectively, and used to transform procyclic parasites with an
329 Amaxa Nucleofector (Lonza)³⁶. After 24h, transfected cells were selected by the addition of
330 blasticidin or puromycin (10µg/ml). After one week, the population was examined (i) for red
331 fluorescence by fluorescence microscopy and (ii) for both red fluorescence and bioluminescence by
332 using a fluorimeter Infinite® 200 (Tecan). Cells were sub-cloned by limiting dilution, and clone
333 selection was performed after 15 days by measuring both bioluminescence in a microplate reader

334 Infinite® 200 (Tecan) and fluorescence with a Muse® cell Analyzer (Merck-Millipore). This strain,
335 named AnTat1.1E AMLuc/tdTomato, was used for natural transmission experiments.
336 The second AnTat 1.1E strain expressing the 3.1 Kb chimeric multiplex reporter protein
337 PpyRE9H::TY1::tdTomato was named AnTat 1.1E AMLuc/TY1/tdTomato. This cytoplasmic reporter
338 is composed of three distinct markers: the red-shifted luciferase (PpyRE9H) is fused to the
339 tdTomato red fluorescent protein by a TY1 tag. Briefly, the 1.68 Kb optimised version of the North
340 American firefly *Photinus pyralis* luciferase³⁷ was fused with a 10-bp sequence known as TY1-tag³⁸
341 and cloned into the pTSARib plasmid³⁵ by using *XhoI* and *HindIII* restriction enzymes to obtain the
342 pTSARib-PpyRE9H-TY1 plasmid. Finally, the 1.4 Kb coding region of the tdTomato fluorescent
343 protein was inserted downstream using *HindIII* and *BamHI*. The resulting 8.9 Kb vector, containing a
344 blasticidin S resistance cassette, was linearised with *SphI* to integrate the rDNA promoter locus.
345 Bloodstream parasites were transformed with an Amaxa Nucleofector (Lonza)³⁶, sub-cloned by
346 limiting dilution, and clone selection was performed by measuring both bioluminescence in a
347 microplate reader Infinite® 200 (Tecan) and fluorescence with a Muse® cell Analyzer (Merck-
348 Millipore). The selected AnTat 1.1E AMLuc/TY1/tdTomato sub-clone was comparable to the
349 parental wild-type strain in terms of growth rate (Table 1-source data 1A), pleomorphism (Table 1-
350 source data 4C), tsetse infectivity and virulence in mice (Table 1-source data 2). In order to verify
351 the reliability of the bioluminescent marker as well as to define the bioluminescence detection
352 threshold of the AnTat 1.1E AMLuc/TY1/tdTomato selected sub-clone, a parasite density /
353 bioluminescence intensity analysis was performed in 96-micro-well plates with an IVIS® Spectrum
354 imager (Perkin Elmer). Parasite density and bioluminescence intensity were correlated when
355 bioluminescence levels were higher than 10^4 p/s/cm²/sr, corresponding to about 10^3 parasites,
356 allowing estimation of the parasite density from *in vivo* imaging over this threshold (Table 1-source
357 data 1B). This correlation was verified by quantification in a microplate reader Infinite® 200 (Tecan)
358 at the very beginning of the first *in vivo* experiment as well as the end of the last one, demonstrating
359 the stability of the triple reporter expression in the AnTat 1.1E AMLuc/TY1/tdTomato selected sub-
360 clone over time, especially after at least one full *in vivo* parasite cycle in the tsetse fly and the
361 mammalian host (Table 1-source data 1C). This strain was used for xenodiagnosis experiments and
362 quantification of parasite densities.

363

364 **Mouse strains**

365 BALB/c and C57BL/6J mice were used as models for chronic disease³⁹. In addition, to allow for
366 further 3D intravital imaging of the lymphatic and blood systems, C57BL/6J-Flk1-EGFP mice
367 expressing a GFP tagged *Kdr* (*Flk1*) gene encoding the vascular endothelial growth factor receptor
368 2 (VEGFR-2) were used¹⁶.

369 **Ethical statements**

370 This study was conducted under Home Office and SAPO regulations in the UK and in strict
371 accordance with the recommendations from the Guide for the Care and Use of Laboratory Animals
372 of the European Union (European Directive 2010/63/UE) and the French Government. The protocol
373 was approved by the “Comité d'éthique en expérimentation animale de l'Institut Pasteur” CETEA 89
374 (Permit number: 2012-0043 and 2016-0017) and undertaken in compliance with Institut Pasteur
375 Biosafety Committee (protocol CHSCT 12.131).

376

377 **Skin invasion time-course**

378 A total of 36 eight-week old BALB/c mice (Harlan, UK) were inoculated by intra-peritoneal (IP)
379 injection with 10^4 parasites of strain STIB 247. Parasitaemia was assayed on each subsequent day
380 using phase microscopy⁴⁰. Twenty-four uninfected animals served as controls. Every three days for
381 36 days, three infected animals and two uninfected animals were culled and 2cm² skin samples
382 removed from the dorsum. Skin samples were fixed in 10% neutral buffered formalin prior to
383 histological analysis.

384

385 **Natural infections using tsetse flies**

386 Tsetse flies (*Glossina morsitans morsitans*) were maintained, infected and dissected at the Institut
387 Pasteur as described previously⁴¹. Flies were infected with AnTat1.1E AMLuc/tdTomato parasites.
388 Positive flies were selected first by screening the abdominal fluorescence (midgut infection) 15 days
389 after the infective meal, and then by a salivation test (mature salivary gland infection) after one
390 month. Single flies with salivary gland infections were used to infect the abdomen of mice
391 anaesthetised by IP injection of ketamine (Imalgene 1000 at 125mg/kg) and xylazine (Rompun 2%
392 at 12.5mg/kg) and feeding was confirmed by visual observation of the fly abdomen full of blood.
393 Control mice were either not bitten or bitten by uninfected flies. The presence and density of
394 parasites in the blood was determined daily by automated fluorescent cell counting with a Muse
395 cytometer (Merck-Millipore, detection limit $5 \cdot 10^2$ parasites/ml) or by direct examination under a
396 phase microscope with standardised one-use haemocytometers (Hycor Kova, detection limit 10^4
397 parasites/ml), according to the manufacturer's recommendations.

398

399 **Infection for xenodiagnosis**

400 A total of 20 seven-week-old male C57BL/6J Rj mice (Janvier, France) were IP injected with 10^5
401 AnTat 1.1E AMLuc/TY1/tdTomato bloodstream forms. Parasitaemia was assayed daily by
402 automated fluorescent cell counting with a Muse cytometer (Merck-Millipore, detection limit $5 \cdot 10^2$
403 parasites/ml) according to the manufacturer's recommendations.

404 **PAD1/ZFP3 relative expression**

405 Three BALB/c were infected with *T.b. brucei* strain TREU927 and culled at day 11. The mice were
406 perfused and a 2cm² region of skin removed from the flank. Skin sections were lysed using a
407 Qiagen TissueLyzer LT and RNA extracted using a Qiagen RNeasy kit following the manufacturer's
408 instructions. 100ng of RNA from each sample was reverse-transcribed using an Invitrogen
409 Superscript III RT kit. qPCR was performed on each sample using 5µl of cDNA using a protocol and
410 primers validated previously⁴² on an Agilent Technologies Stratagene Mx3005P qPCR machine.
411 The ratio of *PAD1* to *ZFP3*, and hence the proportion of cells transcribing the *PAD1* gene, was
412 estimated using the Agilent Technologies MXPro software.

413 **Xenodiagnosis**

414 Mice were first anaesthetised by IP injection of ketamine (Imalgene 1000 at 125 mg / kg) and
415 xylazine (Rompun 2% at 12.5 mg/kg). Batches of 10 teneral male tsetse flies (from 8 to 24 h post-
416 eclosion) were then placed in 50 ml Falcon tubes closed with a piece of net through which they
417 were allowed to feed directly on mouse skin regions of interest for 10 minutes. The selection of the
418 skin regions for fly feeding was based on mice bioluminescence profiles and parasitaemia. Unfed
419 flies were discarded and fed flies were maintained as previously described. Anaesthetised mice
420 were finally sacrificed by cervical dislocation and their skin was dissected for controlling
421 bioluminescence with an IVIS® Spectrum imager (Perkin Elmer). All the flies were dissected and
422 checked for the presence of trypanosomes either 2 or 14 days after their meal on mouse skin by
423 two entomologists blinded to group assignment and experimental procedures. Dissections were
424 performed as previously described⁴¹, entire midguts were scrutinised by fluorescence microscopy to
425 detect and count living red fluorescent parasites, and positive midguts were further treated for IFA.
426 A total of 420 flies were used in 3 independent xenodiagnosis experiments.

427

428 **In vitro bioluminescence imaging**

429 To perform the parasite density / bioluminescence intensity assay with AnTat 1.1E
430 AMLuc/TY1/tdTomato bloodstream forms, parasites were counted, centrifuged and resuspended in
431 fresh HMI11 medium at 10.10⁶ cells/ml. Then, 100µl (or 10⁶ parasites) of this suspension were
432 transferred into black clear-bottom 96-well plates and serial 2-fold dilutions were performed in
433 triplicate adjusting the final volume to 200µl of HMI11 with 300 µg/ml of beetle luciferin (Promega,
434 France). Luciferase activity was quantified after 10 minutes of incubation with a microplate reader
435 Infinite® 200 (Tecan), following the instructions of the Promega Luciferase Assay System. After
436 background removal, results were analysed as mean ±SD of three independent experiments.

437 ***In vivo* bioluminescence imaging**

438 Infection with bioluminescent parasites was monitored daily by detecting the bioluminescence in
439 whole animals with the IVIS® Spectrum imager (Perkin Elmer). The equipment consists of a cooled
440 charge-coupled camera mounted on a light-tight chamber with a nose cone delivery device to keep
441 the mice anaesthetised during image acquisition with 1.5% isoflurane. D-luciferin potassium salt
442 (Promega) stock solution was prepared in phosphate buffered saline (PBS) at 33.33 mg/ml, filter-
443 sterilised and stored in a -20°C freezer. To produce bioluminescence, mice were inoculated IP with
444 150 µl of D-luciferin stock solution (250mg/kg). After 10 minutes of incubation to allow substrate
445 dissemination, all mice were anaesthetised in an oxygen-rich induction chamber with 2%
446 isoflurane, and images were acquired by using automatic exposure (30 seconds to 5 minutes)
447 depending on signal intensity. Images were analysed with Living Image software version 4.3.1
448 (Perkin Elmer). Data were expressed in average radiance (p/s/cm²/sr) corresponding to the total flux
449 of bioluminescent signal according to the selected area (total body of the mouse here). The
450 background noise was removed by subtracting the bioluminescent signal of the control mouse from
451 the infected ones for each acquisition.

452 **2-photon microscopy**

453 Intravital multi-photon microscopy studies were carried out using a Zeiss LSM7 MP system
454 equipped with a tuneable titanium:sapphire solid-state two-photon excitation source (4W,
455 Chameleon Ultra II, Coherent Laser Group) coupled to an Optical Parametric Oscillator (Chameleon
456 Compact OPO; Coherent). Movies were acquired for 10 to 15 minutes with an X:Y pixel resolution
457 of 512 x 512 in 2µm Z increments producing up to 40µm stacks. 3D tracking was performed using
458 Volocity 6.1.1 (Perkin Elmer, Cambridge, UK). Values representing the mean velocity, displacement
459 and meandering index were calculated for each object. Mice were anaesthetised IP using
460 medetomidine (Domitor 0.5mg/kg) and ketamine (50mg/kg) and placed on a heated stage.
461 Following removal of hair with a depilatory cream, dorsal skin was imaged. An intravenous injection
462 of non-targeted quantum dots (Qdot705) (Life Technologies, UK) prior to imaging allowed
463 visualisation of blood vessels.

464 **Spinning-disk confocal microscopy**

465 AnTat1.1E AMLuc/tdTomato parasites were monitored in the ear of *Kdr (Flk1)* C57BL/6J Rj mice by
466 spinning-disk confocal microscopy as described previously⁴¹. Briefly, mice were first anaesthetised
467 by IP injection of ketamine (Imalgene 1000 at 125mg/kg) and xylazine (Rompun 2% at 12.5mg/kg).
468 Mice were wrapped in a heating blanket and placed on an aluminium platform with a central round
469 opening of 21mm in diameter. A coverslip was taped on the central hole and the mouse was
470 positioned so that the ear was lying on this oiled coverslip. Imaging was performed using an
471 UltraView ERS spinning-disk confocal system (Perkin Elmer) with a x40 oil objective (1.3 numerical
472 aperture). Movies were acquired by an EM-CCD camera (Hamamatsu) controlled by the Volocity

473 software (Perkin Elmer) with an exposure time of 500ms for a total of 30 to 120s. Images were
474 analysed using ImageJ 1.48v and its plugin Bio-formats importer (NIH).

475 **Histological and immunohistochemical evaluation of the skin**

476 Paraformaldehyde-fixed skin samples were trimmed and processed into paraffin blocks. Sections
477 were stained with Haematoxylin and Eosin (HE). Additional serial sections were processed for
478 immunohistochemical staining using a polyclonal rabbit antibody raised against the invariant surface
479 glycoprotein 65 (IGS65) (M. Carrington, Cambridge, UK) using a Dako Autostainer Link 48 (Dako,
480 Denmark) and were subsequently counterstained with Gill's Haematoxylin.

481 **Histopathological assessment of inflammation in the skin**

482 The extent of cutaneous inflammatory cell infiltration was assessed in haematoxylin and eosin
483 stained sections with a semi-quantitative scoring system applied by two pathologists blinded to
484 group assignment and experimental procedures. The extent of mixed inflammatory cell infiltration in
485 the dermis and/or subcutis was assessed on a 0 to 3 grading scale (0 = no inflammation or only few
486 scattered leukocytes; 1 = low numbers of inflammatory cells; 2 = moderate numbers of inflammatory
487 cells; 3 = large numbers of inflammatory cells). Ten high-power fields were scored for each skin
488 sample. An inflammation score calculated as the average of the scores in the 10 high-power fields
489 was determined for each sample.

490 **Semi-quantitative evaluation of the parasite burden in skin sections**

491 Parasite burden was assessed in skin sections stained with anti-IGS65 antibody by two pathologists
492 blinded to group assignment and experimental procedures. Presence of parasites defined as
493 intravascular (parasites within the lumen of dermal or subcutaneous small to medium-sized vessels)
494 and extravascular (parasites located outside blood vessels, scattered in the connective tissue of the
495 dermis or in the subcutis) was evaluated in 5 randomly selected high-power fields at x40
496 magnification with a 0 to 3 semi-quantitative grading scale (0 = no parasites detectable; 1 = low
497 numbers of parasites (< 20); 2 = moderate numbers of parasites (20 < 50); 3 = large numbers of
498 parasites (> 50). An average parasite burden score was calculated for each sample.

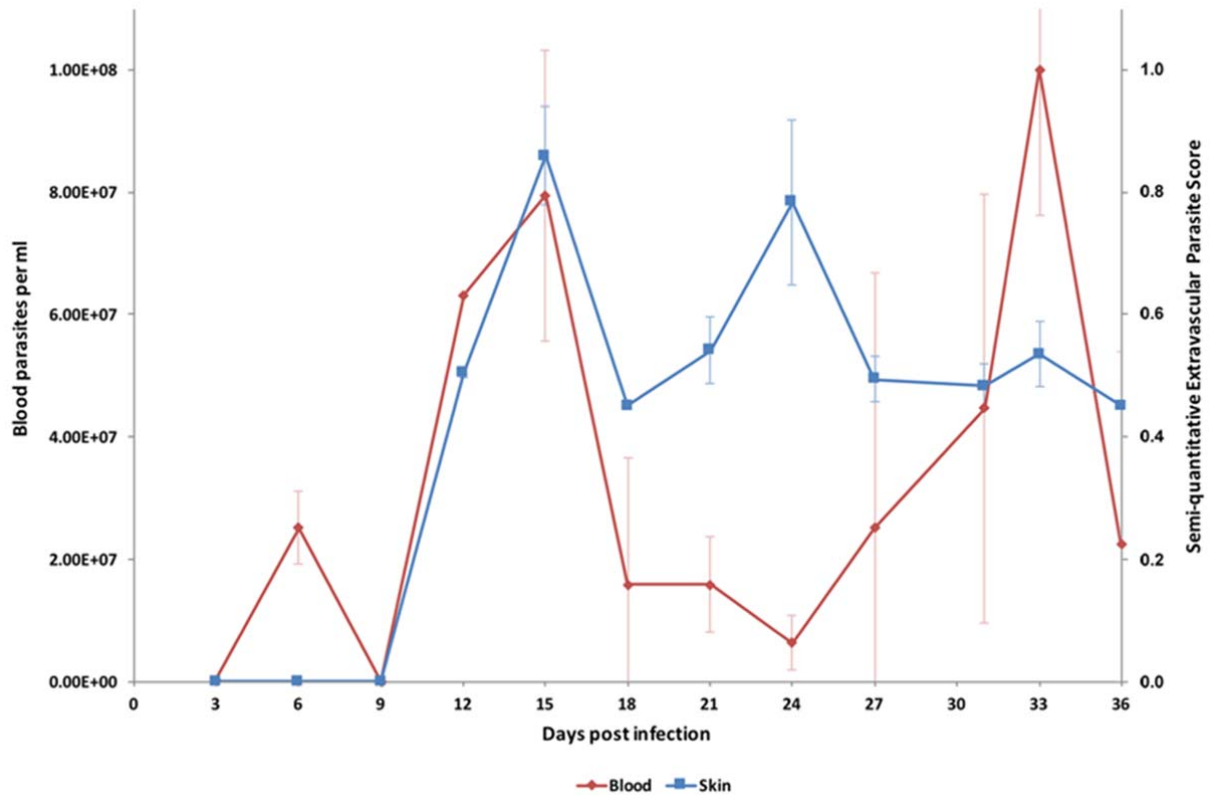
499 **Immunofluorescence analysis**

500 Cells were treated for immunofluorescence after paraformaldehyde or methanol fixation as
501 described previously¹⁷. Parasites were stained with one or two of the following antibodies: (i) the
502 anti-CRD polyclonal rabbit antibody (1:300) to label the cross-reactive determinant of the
503 glycosylphosphatidylinositol anchors of proteins, predominantly the variant surface glycoproteins⁴³,
504 (ii) the anti-PAD1 polyclonal rabbit antibody (1:100) targeting the carboxylate-transporter Proteins
505 Associated with Differentiation 1 (PAD1) (Keith Matthews, Edinburgh, UK)¹⁷, (iii) the anti-GPEET
506 mouse IgG3 monoclonal antibody (1:500) targeting the *T. brucei* GPEET-rich procyclin (Acris
507 Antibodies GmbH, San Diego, USA), (iv) the L8C4 mouse IgG1 monoclonal antibody labelling an

508 epitope of the PFR2 protein⁴⁴. Specific antibodies with minimal cross-reactions with mice and
509 coupled to AlexaFluor 488, Cy3 or Cy5 (Jackson ImmunoResearch, USA) were used as secondary
510 antibodies. DNA was stained with 4,6-diamidino-2-phenylindole (DAPI). IFA image acquisition was
511 carried out on a Leica 4000B microscope with a x100 objective lens using a Hamamatsu ORCA-
512 03G camera controlled by Micro-manager and images were normalised and analysed with ImageJ
513 1.49v (NIH).

514 **Histopathology of Historical Human Skin Samples**

515 Historical human skin samples were collected from 1991 to 1995 as part of The National
516 Onchocerciasis Task Force (NOTF)⁴⁵. Of this collection, 1,121 paraffin embedded skin samples
517 were cut into 2.5 micron sections and stained with Giemsa (Sigma-Aldrich). Slides were screened
518 for the presence of parasites by two pathologists independently and representative images taken at
519 x100 magnification.

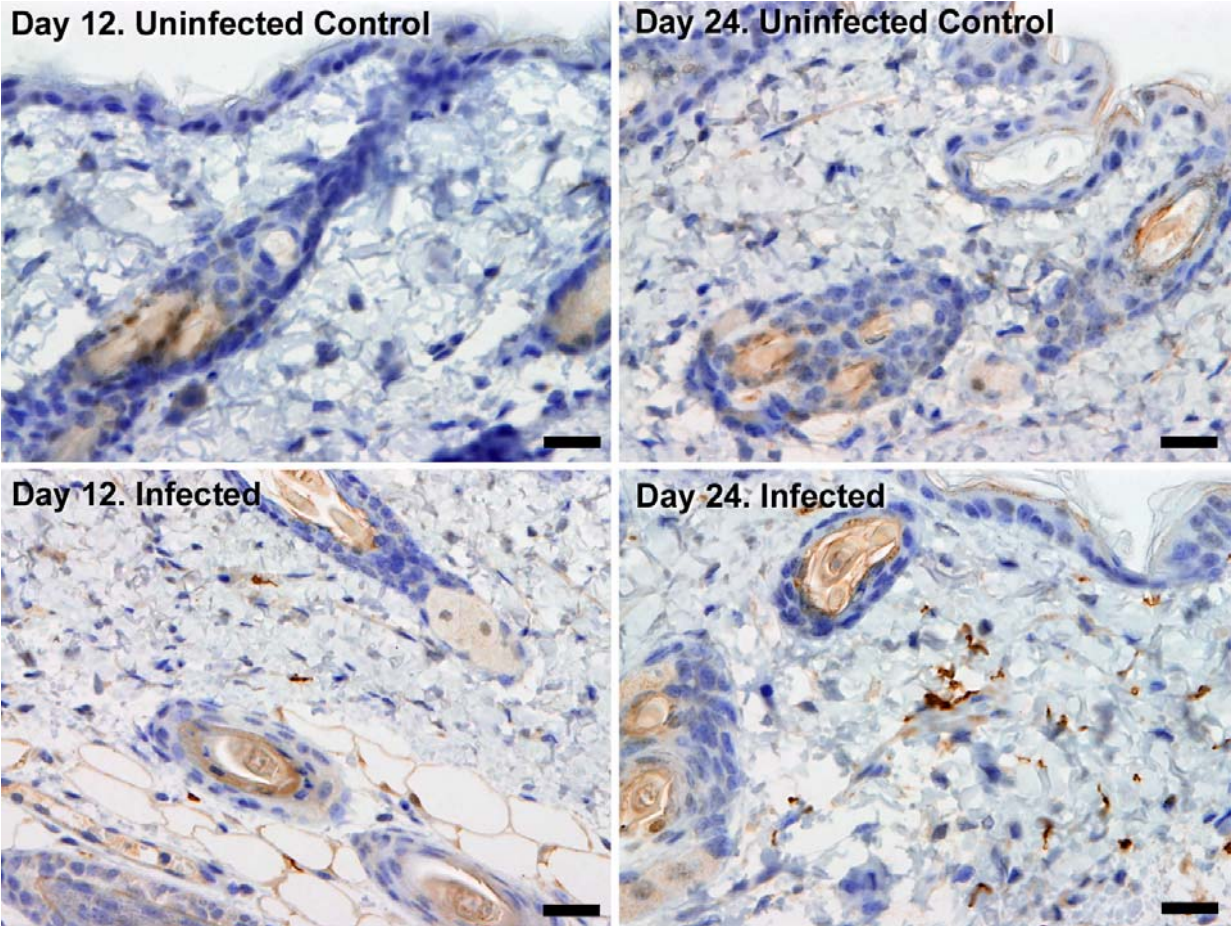


520

521 **Figure 1. Parasite densities in the blood and in the extravascular tissue of the skin over a**
 522 **time-course**

523 The blood parasitaemia of *T.b. brucei* strain STIB247 (red) and the semi-quantitative score of
 524 extravascular parasites in the skin (blue) are shown over a 36-day time-course following infection in
 525 Balb/C mice. Blood parasitaemia was measured using phase microscopy using methodology
 526 outlined in ⁴⁰. Skin parasite burden is an average of five high-power fields scored by histological
 527 analysis (0 = no parasites detectable; 1 = low numbers of parasites; 2 = moderate numbers of
 528 parasites; 3 = large numbers of parasites). Standard error shown (n=3).

529

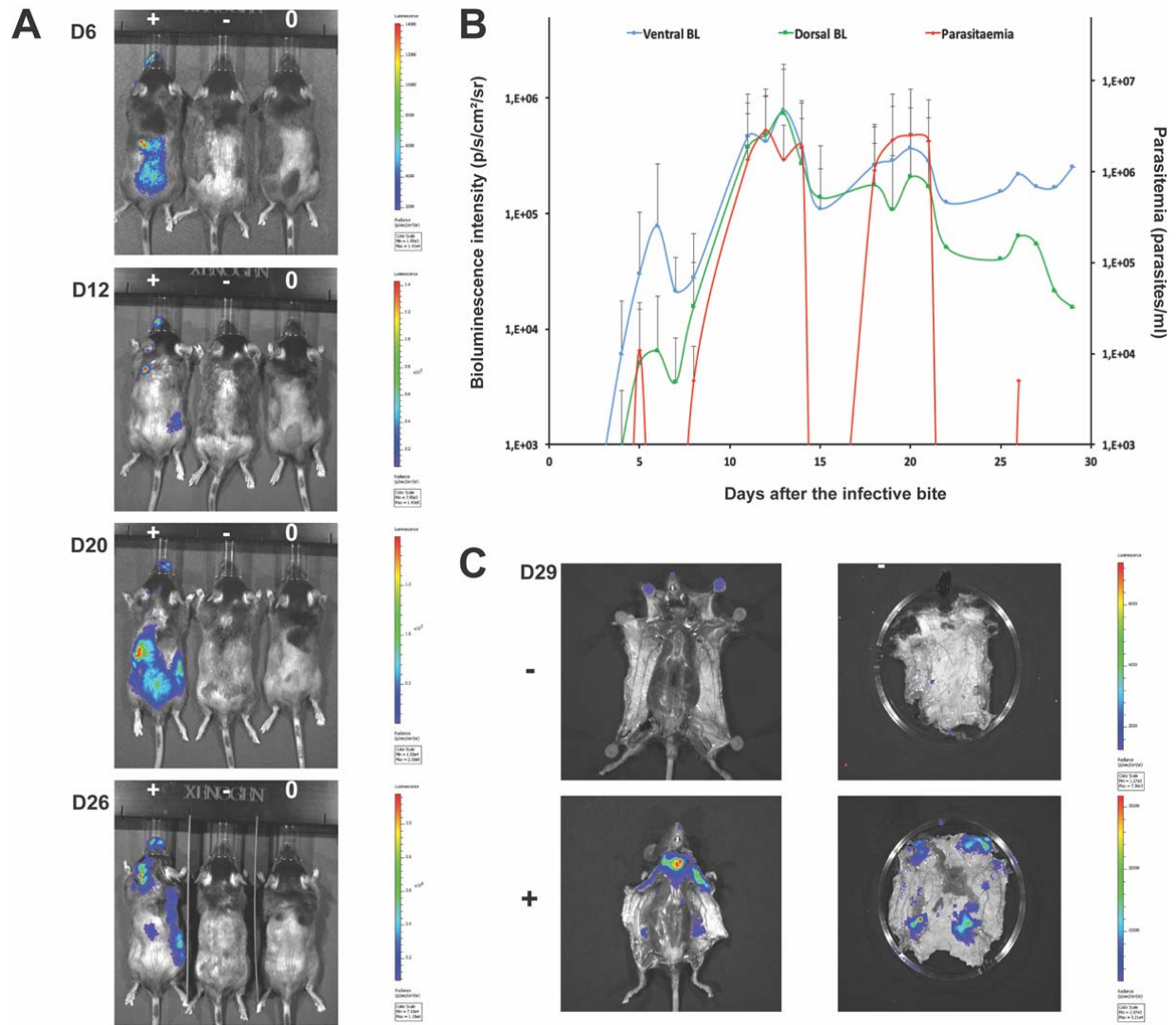


530

531 **Figure 2. Extravascular localisation of trypanosomes during an infection**

532 Histological sections of dorsal skin from uninfected and infected Balb/C mice stained with
533 trypanosome-specific anti-ISG65 antibody (brown), counterstained with Gill's Haematoxylin stain
534 (blue) at 12 days and 24 days post-inoculation with *T.b. brucei* strain STIB247. Parasites are visible
535 in extravascular locations of the skin including the deep dermis and subcutaneous adipose tissue
536 from day 12. The scale bar represents 20µm.

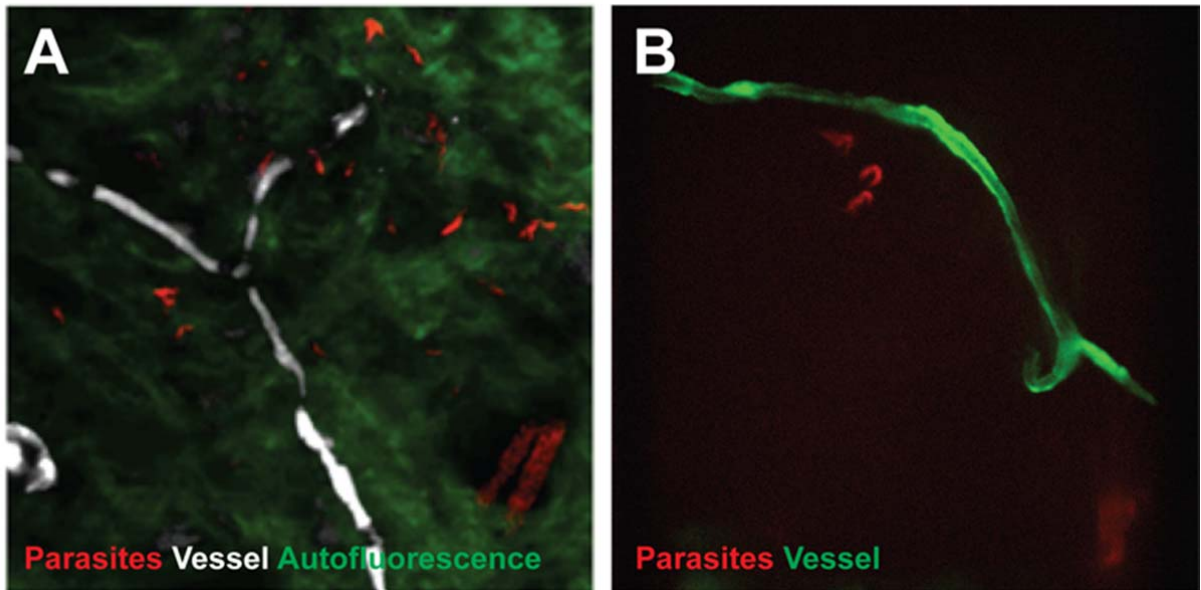
537



538

539 **Figure 3. Dynamics of parasite distribution in the extravascular tissue of the skin and in the**
 540 **blood during a representative course of infection following natural transmission**

541 A total of seven mice were infected by the single infective bite of an individual *G.m. morsitans* on
 542 the belly with the *T.b. brucei* AnTat1.1E AMLuc/tdTomato strain. Panels A and C depict
 543 representative patterns. (A) Examples of bioluminescence profiles of 3 mice (+ bitten by an infected
 544 fly, - bitten by an uninfected fly and 0 not bitten) 6, 12, 20 and 26 days after the bite are shown. (B)
 545 Ventral (blue) and dorsal (green) bioluminescence (BL) intensities (in p/s/cm²/sr on the left Y-axis)
 546 and parasitaemia (in parasites/ml in red on the right Y-axis) were measured daily for 29 days and
 547 plotted as mean \pm SD (n=7 mice). (C) The entire skins of mice (+) and (-) were dissected for
 548 bioluminescence imaging 29 days after the bite. For the mouse (+), Figure 3–figure supplement 1
 549 shows the bioluminescence profile of dissected organs, Figure 3–figure supplement 2 presents the
 550 skin inflammation, and Figure 3–figure supplement 3 shows labelled parasites in skin sections.



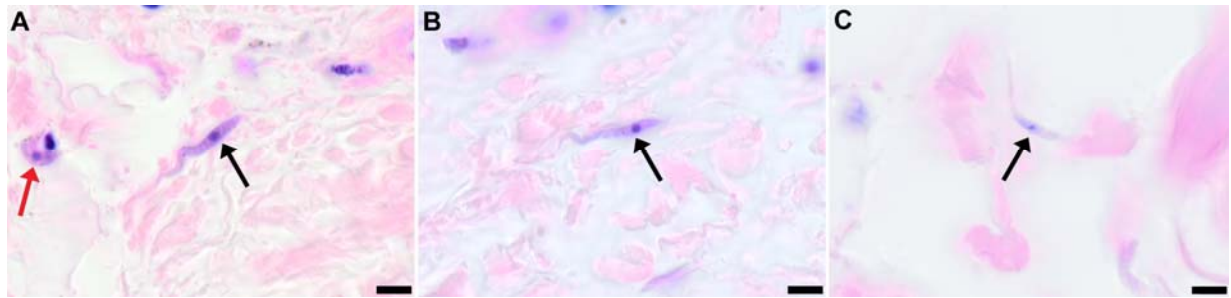
551

552 **Figure 4. Extravascular localisation of trypanosomes during an infection visualised using**
 553 **multi-photon microscopy (A) and spinning-disk confocal microscopy (B)**

554 (A) Still-image extracted from video (Video 1) of multi-photon live imaging of dorsal skin during a
 555 trypanosome infection. Intravenous non-targeted quantum dots (white) highlight blood vessels. *T.b.*
 556 *brucei* STIB 247 parasites transfected with mCherry to aid visualisation (red) are clearly visible and
 557 motile outside the vasculature and within the extravascular skin matrix (green). (B) Still-image
 558 extracted from (Video 3) of spinning-disk confocal live imaging of the ear of an *Kdr (Flk1)* C57BL/6J
 559 Rj mouse during a trypanosome infection. *T.b. brucei* AnTat1.1E AMLuc/tdTomato parasites
 560 expressing tdTomato (red) are moving in the extravascular region surrounding a vessel of the
 561 dermis (green).

562

563



564

565 **Figure 5. Extravascular localisation of trypanosomes in previously unidentified human cases**
566 **of trypanosomiasis**

567 Histological sections of skin collected from previously unidentified cases of human trypanosomiasis
568 from the Democratic Republic of Congo, showing the presence of extravascular parasites in
569 biopsies from three individuals (A, B and C). Skin biopsies were collected as part of a national
570 onchocerciasis screening programme that took place in the same geographic region as an active
571 trypanosomiasis focus. Slides were stained with Giemsa and examined under oil immersion at 100x
572 magnification. In addition to visible slender forms (black arrows) in the extravascular tissue of the
573 skin, a clearly identifiable stumpy transmission form with typical morphology and an unattached
574 undulating membrane is also present in the skin of one individual (red arrow in A). The scale bar
575 represents 5µm.

576

Fly batches	Parasites in blood (per ml)	Parasites in skin (per cm ²)	Dissected flies	Fly infection rates (%)
C1	0	0	32	0%
C	0	0	8	0%
A4B	< 10 ⁴	< 10 ³	16	0%
B1B	2.2x10 ⁴	< 10 ³	13	0%
A4A	< 10 ⁴	6.6x10 ⁵	17	35%
A2A	1.1x10 ⁴	3.8x10 ⁶	7	86%
B1A	2.2x10 ⁴	4.6x10 ⁷	16	31%
3B	4.4x10 ⁴	2.6x10 ⁴	14	36%
3A	4.4x10 ⁴	2.6x10 ⁴	16	38%
1B	1.8x10 ⁵	8.0x10 ³	12	67%
1A	1.8x10 ⁵	8.0x10 ³	14	79%
4B	2.2x10 ⁵	1.2x10 ⁴	17	53%
4A	2.2x10 ⁵	1.2x10 ⁴	18	56%
2B	1.6x10 ⁶	8.0x10 ³	14	36%
2A	1.6x10 ⁶	3.2x10 ⁴	18	39%
B4B	4.3x10 ⁶	6.7x10 ⁷	10	80%
B4A	4.3x10 ⁶	6.7x10 ⁷	17	100%

577

578 **Table 1. Skin parasites are ingested during tsetse pool-feeding**

579 Mice were IP infected with *T.b. brucei* AnTat1.1E AMLuc/TY1/tdTomato and the parasitaemia and
580 bioluminescence were monitored daily until the day of xenodiagnosis. The number of parasites in
581 the blood was determined using a haemocytometer or a flux cytometer. The number of parasites in
582 the skin was estimated from the measured bioluminescence intensity by using a standard curve
583 (Table 1-source data 1 and Table 1-source data 2). Batches of teneral flies were fed on different
584 skin regions of mice infected with differing levels of bioluminescence across the skin and with
585 differing levels of parasitaemia (Table 1-source data 2 and Table 1-source data 3). Fly batches A4A,
586 A2A, B1A, 3B and 3A were used to assess tsetse transmission in hosts with low numbers of blood
587 parasites but high numbers skin parasites, while fly batches 1B, 1A, 4B, 4A, 2B, 2A, B2B and B4A
588 were used to investigate the impact of high numbers of parasites in both the skin and blood. Flies
589 were dissected and their midguts checked for the presence of fluorescent trypanosomes after two
590 days to determine the proportion of infected flies (Table 1-source data 4A-B). For some of these
591 experiments, results of an in-depth quantification of parasite stages by IFA is provided in
592 Supplementary file 4. Stumpy forms were observed only in the blood of mice with parasitaemia
593 values highlighted in light grey. Bioluminescence was detected in the skin of mice with values
594 highlighted in dark grey.

595 **Figure Supplements**

596

597 **Figure 2-figure supplement 1. Skin invasion by *T.b. brucei* strain TREU927 and *T.b.***
598 ***gambiense* strain PA**

599 Histological sections of dorsal skin from a mouse infected with *T.b. brucei* strain TREU927 at 20x
600 magnification and two mice infected with *T.b. gambiense* strain PA at 40x magnification 10-days
601 post-inoculation. Trypanosome-specific anti-ISG65 antibody reveals the presence of extravascular
602 parasites (brown) and the slides were counterstained with Gill's Haematoxylin stain (blue) to reveal
603 host skin structure.

604

605 **Figure 3-figure supplement 1. Bioluminescence mostly originates from parasites in the skin**

606 Mouse (+) was sacrificed and dissected for bioluminescence imaging 29 days after the infective
607 bite. Fig 3C shows the bioluminescence profile of its entire skin and dissected organs are shown
608 here.

609

610 **Figure 3-figure supplement 2. Mild inflammation of skin tissues one month after an infection**
611 **by natural transmission**

612 After 29 days, the most bioluminescent skin region of mouse (+) was dissected, fixed in
613 paraformaldehyde, embedded in paraffin and stained with HE. Multifocal inflammatory infiltrates
614 containing neutrophils were located in the dermis and subcutaneous tissue and associated with
615 oedema. Inflammatory foci were generally centred on blood vessels (arrows).

616

617 **Figure 3-figure supplement 3. Extravascular parasites in the skin express both VSGs and**
618 **PAD1 surface markers**

619 After 29 days, the most bioluminescent skin region of mouse (+) was dissected, fixed in
620 paraformaldehyde, embedded in paraffin and treated for IFA with the anti-CRD antibody that
621 predominately labels parasites expressing VSGs (A-B), or the anti-PAD1 antibody specific to
622 transmission form "stumpy" cells (C-D).

623 **Source Data**

624

625 **Table 1-source data 1. Characterisation of the AnTat 1.1E AMLuc/TY1/tdTomato sub-clone**

626 (A) The *in vitro* growth of the selected AnTat1.1E AMLuc/TY1/tdTomato sub-clone (red) was similar
627 to that of the parental wild-type strain (blue). Bloodstream forms were cultured in HMI11, counted
628 daily in a Muse cytometer (Merck-Millipore) and diluted after 4 days. (B) A parasite density /
629 bioluminescence intensity analysis was performed by measuring the bioluminescence in successive
630 2-fold dilutions in 96-micro-well plates with an IVIS® Spectrum imager (Perkin Elmer). When plotted
631 as mean \pm SD (n=3), parasite densities and bioluminescence intensities were correlated when the
632 bioluminescence levels were higher than 10^4 p/s/cm²/sr, corresponding to about 10^3 parasites,
633 allowing estimation of the parasite density from *in vivo* imaging over this threshold. This standard
634 curve was used to estimate the number of parasites in the skin from measured values of
635 bioluminescence. (C) This correlation was verified by quantification in a microplate reader Infinite®
636 200 (Tecan) at the very beginning of the first *in vivo* experiment as well as the end of the last one
637 (mean \pm SD, n=3).

638

639 **Table 1-source data 2. Parasite densities in extravascular tissue of the skin and in the blood**
640 **of mice used for differential xenodiagnosis**

641 Mice were injected IP with AnTat1.1E AMLuc/TY1/tdTomato and monitored daily for
642 bioluminescence and parasitaemia. (A) Bioluminescence profile of four mice (- uninfected control
643 and (1-3) three infected mice) four days after infection. (B) The entire skins of the uninfected control
644 mouse (-) and mouse 3 were dissected for bioluminescence imaging four days after infection. (C)
645 Parasite densities in the blood and in the skin (calculated from the mean dorsal bioluminescence
646 intensity measurement and from the standard curve in Figure 4-figure supplement 3B, in
647 parasites/cm² in blue) were calculated daily over one week and plotted as mean \pm SD (n=13 mice).

648 **Table 1-source data 3. Skin parasites are sufficient to initiate a tsetse infection**

649 Schematics summarising the principal results from the xenodiagnosis experiment. In a mouse with
650 no detected transmissible parasites in the blood (absence of stumpy forms by IFA and absence of
651 infection of flies fed on a non-bioluminescent region of the skin), flies can ingest transmissible
652 parasites from the bioluminescent region of the skin (left panel). When a mouse presents
653 transmissible forms in the blood, fly infection rates increase with the concomitant ingestion of
654 parasites from the skin (right panel). Values correspond to those obtained for mouse A4 and B4.

655

656 **Table 1-source data 4. Parasite stage determination by labelling of specific surface markers**

657 Parasites recovered from infected tsetse midguts (A-B) or included in bloodsmears (C) were fixed in
658 methanol for 5 seconds and stained either with the anti-GPEET antibody detecting early procyclic

659 forms (red in A-B) and the L8C4 antibody labelling the flagellum PFR (green in A-B), or with the
660 anti-PAD1 antibody detecting intermediate and stumpy forms (green in C), respectively.

661

662 **Figure 1-source data 1. Semi-quantitative evaluation of the parasite burden in skin sections**
663 **(STIB247)**

664 Every three days for 36 days of a STIB247 *T.b. brucei* infection, five mice were culled (three
665 infected, two control) and skin sections stained with parasite-specific anti-IGS65 antibody. Parasite
666 burden was assessed by two pathologists blinded to group assignment and experimental
667 procedures. Presence of parasites defined as intravascular (parasites within the lumen of dermal or
668 subcutaneous small to medium-sized vessels) and extravascular (parasites located outside blood
669 vessels, scattered in the connective tissue of the dermis or in the subcutis) was evaluated in 5 high-
670 power fields at x40 magnification with a 0 to 3 semi-quantitative grading scale (0 = no parasites
671 detectable; 1 = low numbers of parasites; 2 = moderate numbers of parasites; 3 = large numbers of
672 parasites).

673

674 **Figure 1-source data 2. Daily parasitaemia during STIB247 infection in Balb/C mice**

675 The daily parasitaemia during a 36-day STIB247 *T.b. brucei* infection was estimated using phase
676 microscopy and methodology outlined in ⁴⁰.

677

678 **Supplementary Files**

679

680 **Supplementary File 1. Histopathological assessment of inflammation in the skin during**
681 **STIB247 infection**

682 The extent of cutaneous inflammatory cell infiltration during the 36-day STIB247 experiment was
683 assessed on haematoxylin and eosin stained sections with a semi-quantitative scoring system
684 applied by two pathologists blinded to group assignment and experimental procedures. The extent
685 of mixed inflammatory cell infiltration in the dermis and/or subcutis was assessed on a 0 to 3
686 grading scale (0 = no inflammation or only few scattered leukocytes; 1 = low numbers of
687 inflammatory cells; 2 = moderate numbers of inflammatory cells; 3 = large numbers of inflammatory
688 cells). Ten high-power fields (HPFs) were scored for each skin sample.

689

690 **Supplementary File 2. Histopathological assessment of inflammation in the skin during**
691 **TREU927 infection**

692 The extent of cutaneous inflammatory cell infiltration at day 10 of infection by strain TREU927
693 experiment was assessed on haematoxylin and eosin stained sections with a semi-quantitative
694 scoring system applied by two pathologists blinded to group assignment and experimental
695 procedures. The extent of mixed inflammatory cell infiltration in the dermis and/or subcutis was
696 assessed on a 0 to 3 grading scale (0 = no inflammation or only few scattered leukocytes; 1 = low
697 numbers of inflammatory cells; 2 = moderate numbers of inflammatory cells; 3 = large numbers of
698 inflammatory cells). Ten high-power fields (HPFs) were scored for each skin sample.

699

700 **Supplementary File 3. Expression of PAD1 relative to ZFP3**

701 The relative abundance stumpy cells in the skin of three BALB/c was estimated using qPCR at day
702 11 post-inoculation with *T.b. brucei* strain TREU927. Mice were culled and perfused to remove
703 blood parasites and a 2cm² region of skin removed from the flank. The tissue was homogenised and
704 RNA extracted. 100ng of RNA from each sample was reverse-transcribed and qPCR performed to
705 estimate the cycle thresholds (C_T) of the stumpy marker PAD1 and the endogenous control ZFP3.
706 As C_T is inversely proportional to amount of target cDNA in the sample and PAD1 and ZFP3 have
707 similar qPCR efficiencies, a comparison of the delta (Δ) of C_T between PAD1 and ZFP3 transcripts
708 reveals the relative ratio of PAD1 to ZFP3 transcripts and hence the proportion of differentiated
709 parasites transcribing the PAD1 gene.

710

711 **Supplementary File 4. Both the respective densities and the proportions of transmissible**
712 **forms of parasites in the skin and in the blood govern the tsetse infection rates during pool**
713 **feeding**

714 For some of the xenodiagnosis experiments shown in Table 1, identification and quantification of

715 parasite stages was performed by IFA on blood smears and skin sections. Stumpy forms were
716 observed only in the blood of mice with parasitaemia values highlighted in light grey.
717 Bioluminescence was detected in the skin of mice with values highlighted in dark grey. The number
718 of parasites in the skin was calculated according to the values obtained in the standard *in vitro*
719 assay (Table 1-source data 1) and is therefore probably an underestimate. Tsetse flies were
720 dissected 2 days after xenodiagnosis. Populations of intermediate and stumpy form cells were
721 assessed in blood smears and in successive skin sections stained either with the anti-CRD antibody
722 or the anti-PAD1 antibody (see Method section). Populations of early procyclic cells were assessed
723 in dissected fly midguts stained with the anti-GPEET antibody (see Method section). ND: not
724 determined.

725

726 **Video 1. Extravascular trypanosomes visualised in the skin using 2-photon microscopy**

727 Intravital multi-photon imaging of the flank skin during trypanosome infection 10 days after IP
728 inoculation. An intravenous injection of non-targeted quantum dots prior to imaging allowed
729 visualisation of blood vessels. mCherry STIB247 *T.b. brucei* parasites (red) are observed moving in
730 the extravascular region surrounding blood vessels of the dermis (white). Collagen auto-
731 fluorescence is visible as green.

732

733 **Videos 2-4. Extravascular trypanosomes visualised in the skin using spinning-disk confocal** 734 **microscopy**

735 Spinning-disk confocal live imaging of the ear of an *Kdr (Flk1)* C57BL/6J Rj mouse during a
736 trypanosome infection after natural transmission. *T.b. brucei* AnTat1.1E AMLuc/tdTomato parasites
737 expressing tdTomato (red) are observed moving in the extravascular region surrounding blood and /
738 or lymphatic vessels of the dermis (green).

739

740

741

742